Performance Analysis of Adaptive Variable Exponent Based Total Variation Image Regularization Algorithm

V. Kamalaveni, S. Veni, K. A. Narayanankuttty

▶ **To cite this version:**

V. Kamalaveni, S. Veni, K. A. Narayanankuttty. Performance Analysis of Adaptive Variable Exponent Based Total Variation Image Regularization Algorithm. 6th International Conference on Computer, Communication, and Signal Processing (ICCCSP), Feb 2022, Chennai, India. pp.128-150, 10.1007/978-3-031-11633-9_11 . hal-04388169

HAL Id: hal-04388169

https://inria.hal.science/hal-04388169v1

Submitted on 11 Jan 2024

HAL is a multi-disciplinary open access archive for the deposit and dissemination of scientific research documents, whether they are published or not. The documents may come from teaching and research institutions in France or abroad, or from public or private research centers.

L'archive ouverte pluridisciplinaire **HAL**, est destinée au dépôt et à la diffusion de documents scientifiques de niveau recherche, publiés ou non, émanant des établissements d'enseignement et de recherche français ou étrangers, des laboratoires publics ou privés.

Distributed under a Creative Commons Attribution 4.0 International License

This document is the original author manuscript of a paper submitted to an IFIP conference proceedings or other IFIP publication by Springer Nature. As such, there may be some differences in the official published version of the paper. Such differences, if any, are usually due to reformatting during preparation for publication or minor corrections made by the author(s) during final proofreading of the publication manuscript.

Performance Analysis of Adaptive Variable exponent Based Total Variation Image Regularization Algorithm

V. Kamalaveni[1*[0000-0001-5054-280x]] S.Veni[2[0000-0002-1070-8219]] and K.A. Narayanankuttty[3[0000-0003-4686-8502]]

[1]Department of Electronics and Communication Engineering, Amrita School of Engineering, Coimbatore, Amrita Vishwa Vidyapeetham, India
vvkamalaveni@gmail.com
[2]Department of Electronics and Communication Engineering, Amrita School of Engineering, Coimbatore, Amrita Vishwa Vidyapeetham, India
s_veni@cb.amrita.edu
[3] Amrita School of Engineering, Coimbatore, Amrita Vishwa Vidyapeetham, India
ka_narayanankutty@yahoo.com

Abstract. In this paper, a new adaptive variable exponent based total variation image regularization algorithm is proposed. In the proposed algorithm a regularizing term based on variable exponent is used. The model adaptively switches between TV-ROF model and Tikhonov model. At the edges the model behaves like a ROF model preserving edges effectively. In the inner region the model behaves like a Tikhonov model which enables strong smoothing. The weight of the fidelity term is also adaptive. The weight is large at edges and small in the constant flat area. In this paper the performance of proposed adaptive variable exponent based total variation model is compared with TV-ROF model and Tikhonov model. The performance of the proposed model is compared with other classical diffusion algorithms such as perona-malik model and self-snake model. In addition the proposed model is also compared with nonlocal means filter. The performance of the proposed algorithm is validated by denoising rician noise corrupted brain magnetic resonance images as well as denoising salt and pepper noise corrupted standard images.

Keywords: Total Variation, Adaptive model, Tikhonov model, TV-ROF model, Variable exponent

1.Introduction and Related Work

Images are often corrupted by noise during acquisition and transmission and so image denoising becomes one of the most essential tasks in image processing applications. The objective of image denoising is to remove noise in the image by protecting edges and fine-scale details. During past two decades mathematical techniques such as partial differential equation (PDE) models and variational models have been used for image denoising [1]. Most popularly used variational model is total variation regularization also known as TV-ROF model. While total variation based regularization can able to minimize noise and also regularize the edges, it has some undesirable properties. The undesirable properties are as follows. Loss of contrast , Loss of Geometry, Loss of Texture and Staircase Effect- this refers to the concept that the denoised image may have blocky regions that is piecewise constant regions[2][3].

To overcome the drawbacks associated with total variation regularization different variational regularization models have been proposed. Among several variational models two models used for contrasting purposes are Tikhonov model and TV-ROF model. Tikhonov model is used for smoothing flat region and TV-ROF model is used for edge preservation. The TV-ROF model can remove noise properly and produce sharper edges. But it introduces staircase effect in the constant uniform areas or flat regions[4][5]. Considering the drawbacks of TV-ROF model many improvements have been suggested by different researchers. To overcome the loss of contrast and texture an iterative regularization method for ROF model was proposed by Osher et al.[6] Another improvement to ROF model is squared L2 norm in the fidelity term is replaced by L1 norm[7][8][17][19].Yet another improvement is spatially varying fidelity term was used to preserve texture and contrast[9][10][11].

The tikhonov regularization can minimize staircase effect but it blurs the edges. To bring a balance between tikhonov model and TV-ROF model that is to avoid staircase effect and protect edges and fine details, we introduce new adaptive variable exponent based total variation model which behaves like TV-ROF model at edges and behaves like Tikhonov model in the inner region. In this work the brain magnetic resonance(MR) images corrupted by rician noise are taken for experimental analysis. In the proposed adaptive total variation model both regularization term and fidelity term are adaptive which eliminates staircasing effect [12][13].

The paper is written as follows. Section 2 explains in detail the proposed adaptive variable exponent based total variation model, its partial differential equation solution (PDE) and the numerical implementation of PDE.

In section 3 performance of proposed model is analysed in depth and compared with other models. Finally section 4 concludes the paper.

2. Materials and Methods

2.1 Proposed Adaptive Variable Exponent based Total Variation Model

The proposed adaptive local feature driven variable exponent based total variation regularization model is described by the eqn.1 The local feature of an image that is whether the pixel belongs to an edge or flat inner region is determined using an edge stopping function c(|▽u|) [14]. The edge stopping function described by eqn.4 is used in the proposed model. The flowchart in Fig.1 describes steps of proposed algorithm .

$$\min_{u}\{E(u)\} = \min_{u}\int_{\Omega}\left(|\nabla u|^{\alpha(|\nabla u|)} + \frac{1}{2}\beta(|\nabla u|)(u-u_0)^2\right)dxdy \tag{1}$$

In the above mentioned model

$$\alpha(|\nabla u|) = 1 + c(|\nabla u|) \tag{2}$$

$$\beta(|\nabla u|) = \rho(1 - c(|\nabla u|)) \tag{3}$$

$$c(|\nabla u|) = \exp\left(-\left(\frac{|\nabla u|}{k}\right)^2\right) \tag{4}$$

In the eqn.1 E(u) is the energy functional, |▽u| is the magnitude of image gradient, α(|▽u|) is the variable exponent, u is the observed image, u_0 is the original noisy image and β(|▽u|) is the regularization parameter [15]. In eqn.1 the first term in the integration is regularizing term and second term is the fidelity term. In eqn. 2 and eqn.3 c(|▽u|) is the edge stopping function. In the eqn.4 k is the gradient threshold parameter. k decides which are the gradients to be considered as edges. The property of edge stopping function is that it has zero or insignificant value for higher image gradient magnitudes and it has value one wherever image gradient is zero[14][17][18]. The edge stopping function has value in the range from 0 to 1 for different image gradients. In this model the regularising term whose exponent is a variable that is function α(|▽u|) dependent on the image gradient. At image edges the value of the exponent is 1 since value of c(|▽u|) is zero. The regularising term is total variation which is the sum of image gradients across the entire image domain. So the model becomes Rudin-Osher-Fatemi model at edges [20] [21][22] which is more efficient in preserving edges[16][19]. In noisy inner region where the gradient value is low, so the value of c(|▽u|) becomes one. The exponent becomes the value two since value of c(|▽u|) is one. Here square of the gradient is used as regularising term that is l_2 norm so the model becomes the tikhonov model in the inner region which enables strong image smoothing in the flat inner region[16][19].

The regularization parameter [23] [31][32]β(|▽u|) is selected adaptively based on the local feature of an image. At the object boundaries the value of the edge function becomes zero that is where image gradient is high. The value of the regularization parameter β(|▽u|) becomes equal to constant parameter ρ. The parameter ρ can be set to value 0.2 which enables better edge preservation [16]. In the inner region of an image the value of edge function c(|▽u|) becomes a value exactly one or value closer to 1. So the value of the regularization parameter β(|▽u|) becomes much smaller than 0.2 and this causes strong smoothing in the flat inner region. If c(|▽u|) is 0.999 and the parameter ρ is 0.2 then β(|▽u |) becomes 0.0002 which enables strong smoothing. This is proved in our previous work[16].

2.2 Partial Differential Equation Solution of Proposed Adaptive Variational Model

The proposed model is solved using the steepest descent method [4][24][25] and the following partial differential equation 5 is obtained as solution of the proposed model .

$$\frac{\partial u}{\partial t} = \nabla\left(g\left(|\nabla u|\right)\nabla u\right) + \beta\left(|\nabla u|\right)\left(u_0 - u\right) \tag{5}$$

Here $u = u_0$ the original noisy image at time $t = t_0$ and the diffusivity function $g(|\nabla u|)$ is given below.

$$g(|\nabla u|) = \phi'(|\nabla u|)/|\nabla u| \tag{6}$$

$$\phi(|\nabla u|) = |\nabla u|^{\alpha(|\nabla u|)} \tag{7}$$

The orthogonal decomposition [26][27][28] of eqn.5 is given in eqn. 8.

$$\frac{\partial u}{\partial t} = c_\xi u_{\xi\xi} + c_\eta u_{\eta\eta} + \beta\left(|\nabla u|\right)\left(u - u_o\right) \tag{8}$$

$$c_\xi = g(|\nabla u|) \tag{9}$$

$$c_\eta = g'\left(|\nabla u|\right)|\nabla u| + g\left(|\nabla u|\right) \tag{10}$$

$$\frac{\partial u}{\partial t} = \phi''\left(|\nabla u|\right)u_{\eta\eta} + g\left(|\nabla u|\right)u_{\xi\xi} + \beta\left(|\nabla u|\right)\left(u_0 - u\right)$$

(11)

The first term in the eqn.11 describes the amount of diffusion along the normal direction of an image edge and second term describes the amount of diffusion along the edge direction. In our model

$$\phi''(|\nabla u|) = \alpha\left(|\nabla u|\right)\left(\alpha\left(|\nabla u|\right) - 1\right)|\nabla u|^{\alpha(|\nabla u|)-2} \tag{12}$$

$$g\left(|\nabla u|\right) = \alpha\left(|\nabla u|\right)|\nabla u|^{\alpha(|\nabla u|)-2} \tag{13}$$

$$u_{\eta\eta} = \frac{1}{(u_x^2 + u_y^2)}\left(u_{yy}u_y^2 + u_{xx}u_x^2 + 2u_x u_y u_{xy}\right) \tag{14}$$

$$u_{\xi\xi} = \frac{1}{(u_x^2 + u_y^2)}\left(u_{xx}u_y^2 + u_{yy}u_x^2 - 2u_x u_y u_{xy}\right) \tag{15}$$

The eqn. 14 describes directional second derivative along gradient direction and eqn. 15 describes directional second derivative along edge direction. In this model ϕ'' is positive for image gradients corresponding to inner regions or flat regions. This enables a forward diffusion[29] in the flat inner region thus preventing staircasing effect in the flat region.

The proposed model described by eqn.11 can be implemented by means of numerical iterative algorithm given in eqn.16. In eqn. 16 n denotes number of iterations.

$$u_{i,j}^{n+1} = u_{i,j}^n + \Delta t\phi''\left(|\nabla u|\right)_{i,j}^n \left(u_{\eta\eta}\right)_{i,j}^n + \Delta t g\left(|\nabla u|\right)_{i,j}^n \left(u_{\xi\xi}\right)_{i,j}^n + \Delta t\beta\left(|\nabla u|\right)_{i,j}^n \left(u_{i,j}^n - \left(u_o\right)_{i,j}^n\right) \tag{16}$$

3. Experimental Results and Performance Analysis of Proposed Model

Brain MR images of different modalities that is T1, T2, Protein density(PD) weighted from Brain Web database are taken for validation of proposed algorithm. We compared the performance of proposed algorithm

with classical partial differential equation based algorithms namely self-snake diffusion, perona-malik diffusion, non local means algorithm proposed by antoni buades [30] , tikhonov model and total-variation ROF model. Rican noise corrupted brain MR images having noise levels 10% and 15% are denoised using proposed algorithm as well as other classical methods for experimental purpose. The visual quality of processed images of proposed algorithm shows that the algorithm proposed outperforms other conventional methods.

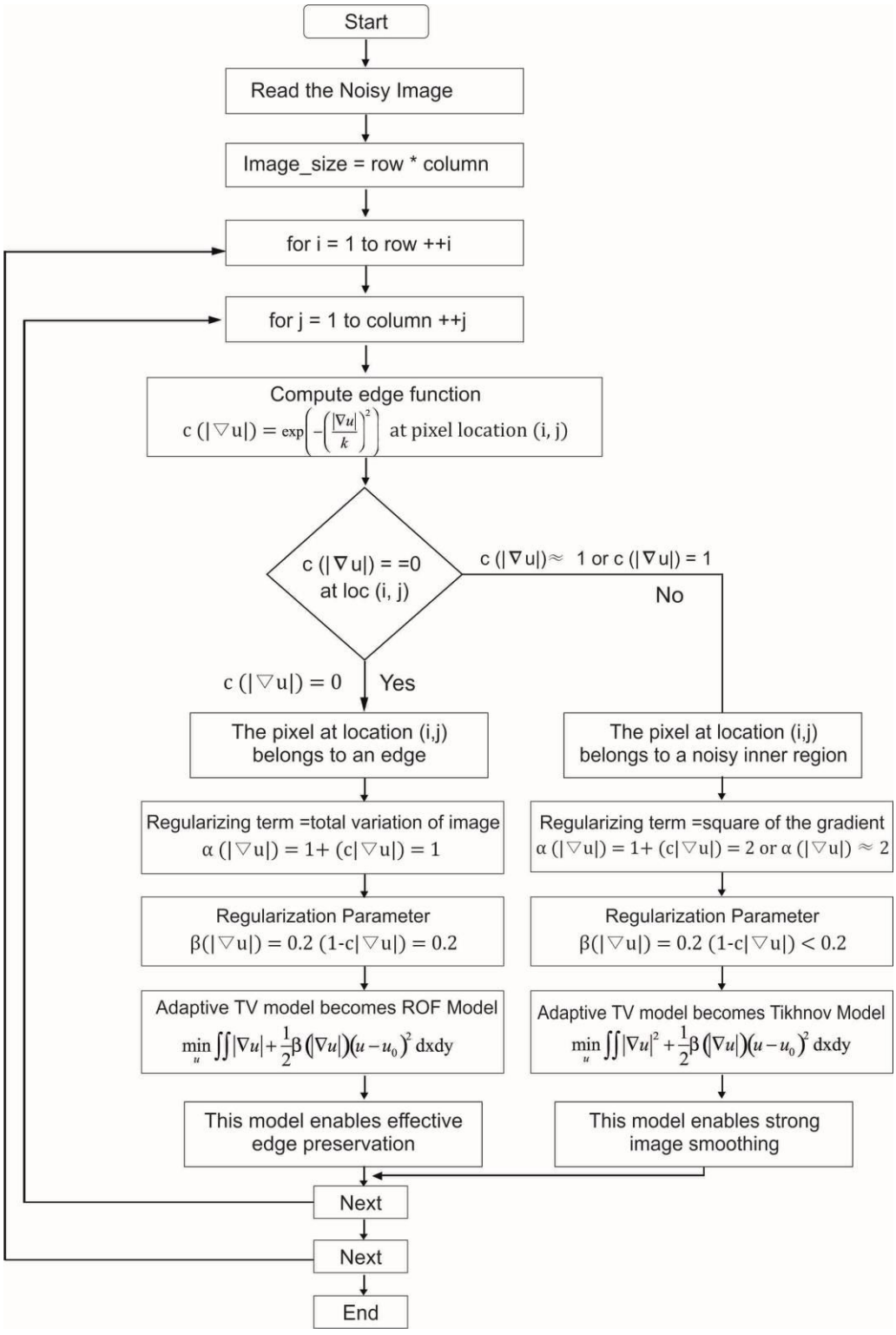

Fig. 1 Flowchart of Proposed Adaptive Variable Exponent based Image Regularization Algorithm

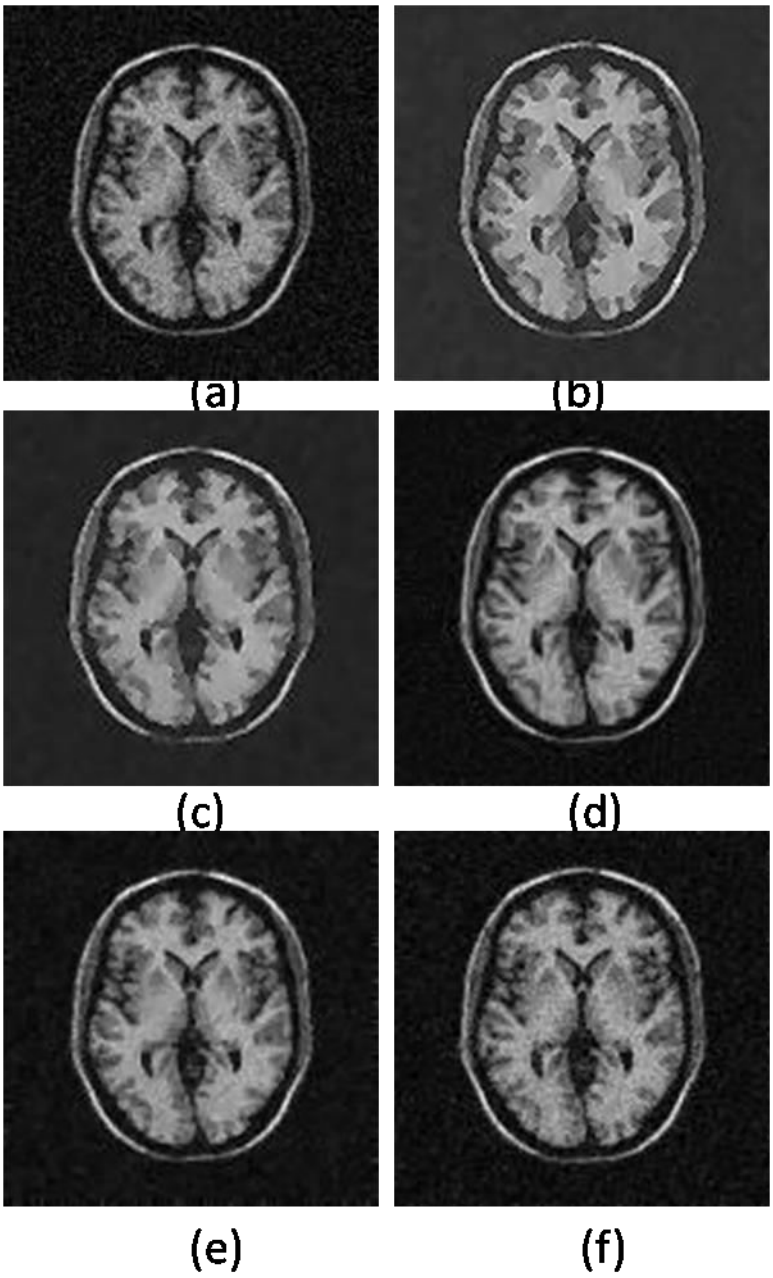

Fig.2 (a) T1-weighted brain MRI slice -55 with 15% noise level (b) denoised image by self-snake model (c) denoised image by perona-malik model (d) denoised image by non-local means algorithm (e) denoised image by TV-ROF (f) denoised image by proposed algorithm.

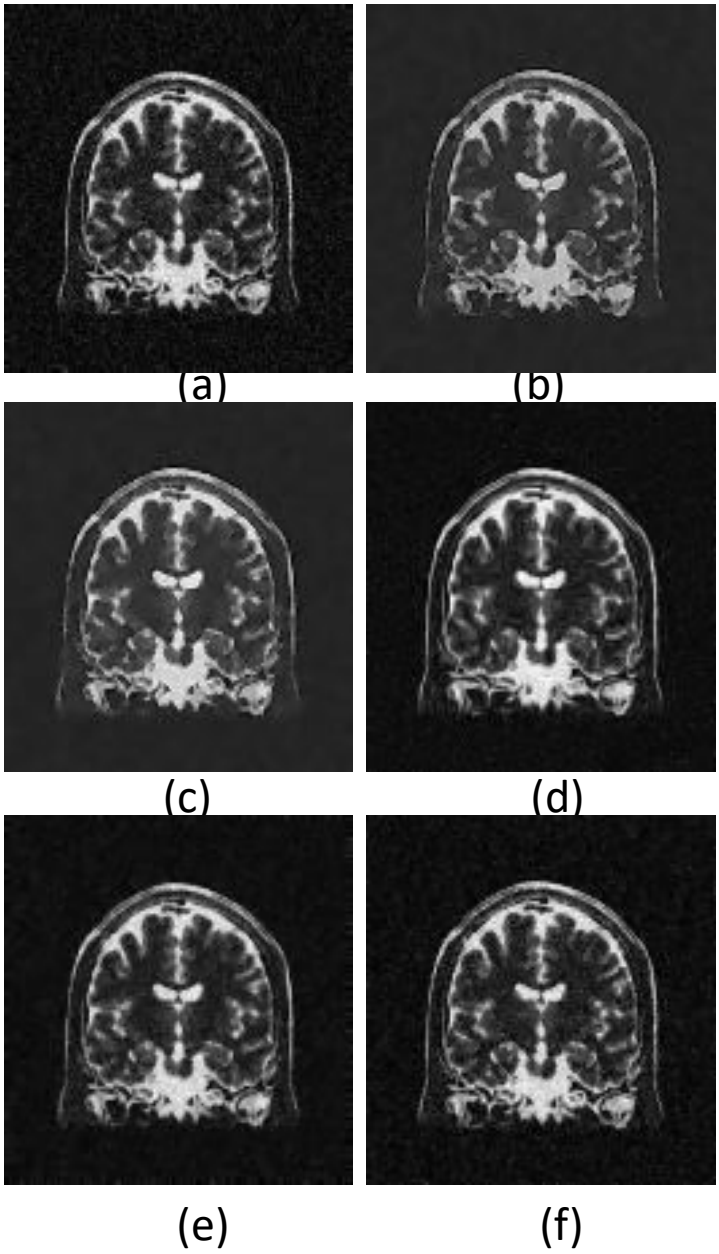

Fig.3 (a) T2-weighted brain MRI coronal slice -67 with 15% noise level (b) denoised image by self-snake model (c) denoised image by perona-malik model (d) denoised image by non-local means algorithm (e) denoised image by TV-ROF (f) denoised image by proposed algorithm.

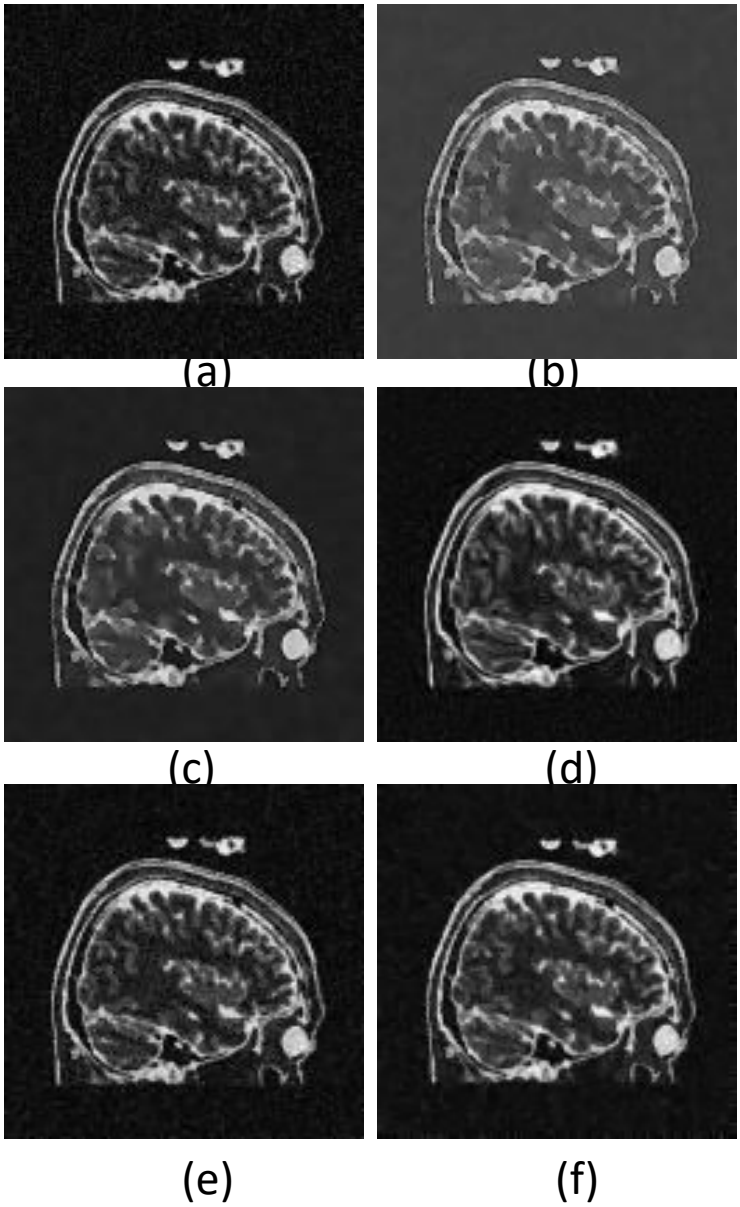

Fig.4 (a) T2-weighted brain MRI sagittal slice -84 with 15% noise level (b) denoised image by self-snake model (c) denoised image by perona-malik model (d) denoised image by non-local means algorithm (e) denoised image by TV-ROF (f) denoised image by proposed algorithm.

The new method is able to produce sharper edges whereas other methods reveal loss of texture, loss of contrast and staircasing. The comparison between visual quality of processed images of different algorithms are shown in Figs.2-4. The quality metrics are computed to evaluate the denoising performance of different algorithms and the values are presented in tables 1-5.

The value of variable exponent $\alpha(|\nabla u|)$ for different values of image gradient is shown in the graph given in Fig.7. Higher image gradients from value 12 onwards the variable exponent takes value one, for threshold parameter k=6. At object boundaries the variable exponent becomes 1 so the model behaves like ROF model preserves edges, contrast and texture very effectively. The value of regularization parameter $\beta(|\nabla u|)$ for different values of image gradient is shown in the graph in Fig.8. Higher image gradients from 12 onwards the regularization parameter takes value 0.2 that is at edges the model takes value 0.2, this value of regularization parameter well preserves edges, object boundaries and texture. The lower image gradients that is gradient value from 1 to 12 the regularisation parameter takes lesser value which enables strong smoothing in the flat region.

TABLE -1 Performance comparison for variable exponent adaptive model, constant exponent -1 ROF model, constant exponent -2 Tikhonov model for rician noise corrupted brain magnetic resonance images.

Modality	Slice/Noise level	Variable exponent-α(.)	SSIM	FSIM	PSNR	MAE
T1-weighted	transverse-55 (10%)	Constant-2 (Tikhonov)	0.7184	0.8296	16.6563	24.2551
	transverse-55 (10%)	Constant-1 (TV-ROF)	0.8620	0.9497	32.8754	4.3333
	transverse-55(10%)	Adaptive Model	0.9127	0.9815	35.1619	3.2415
	transverse-55(15%)	Constant-2 (Tikhnov)	0.6024	0.8035	16.1997	26.4457
	transverse-55(15%)	Constant- 1 (TV-ROF)	0.8462	0.9508	31.3885	5.0586
	transverse-55 (15%)	Adaptive Model	0.9202	0.9804	33.5143	3.7520
T2-weighted	Sagittal-84 (10%)	Constant-2 (Tikhonov)	0.6647	0.7554	20.2204	14.9718
	Sagittal-84 (10%)	Constant-1 (TV-ROF)	0.8585	0.9546	30.9716	4.9697
	Sagittal-84 (10%)	Adaptive Model	0.9124	0.9818	32.1781	4.5780
PD-weighted	transverse-64 (15%)	Constant -2 (Tikhonov)	0.5444	0.7471	19.9165	17.9889
	transverse-64(15%)	Constant-1 (TV-ROF)	0.7967	0.9114	23.2581	13.0546
	transverse-64 (15%)	Adaptive Model	0.9008	0.9658	24.2840	11.7736

TABLE -2 SSIM comparison for perona-malik model, self-snake model, nonlocal means, TV-ROF model and proposed model for rician noise corrupted brain magnetic resonance images.

Modality	Slice/Noise level	Sel-snake	Perona-Malik	Nonlocal means	TV-ROF	Proposed Model
T1-weighted	transverse-55 (10%)	0.6038	0.6697	0.8655	0.8620	0.9127
	transverse-55 (15%)	0.5982	0.6475	0.8735	0.8462	0.9202
T1-weighted	transverse-69 (10%)	0.5977	0.6533	0.8579	0.8421	0.9025
	transverse-69 (15%)	0.5739	0.6040	0.8362	0.8219	0.9019
T2-weighted	Coronal-67 (10%)	0.6289	0.6487	0.8305	0.8310	0.8950
	Coronal-67 (15%)	0.5919	0.6300	0.8441	0.8021	0.8852
T2-weighted	Sagittal-84 (10%)	0.5567	0.6719	0.8550	0.8525	0.9124
	Sagittal-84 (15%)	0.5444	0.6605	0.8541	0.8331	0.9012
PD-weighted	transverse-64 (10%)	0.5515	0.5884	0.8372	0.8308	0.8969
	transverse-64 (15%)	0.5264	0.5403	0.8371	0.7967	0.9008
PD-weighted	Sagittal-64 (10%)	0.4996	0.5798	0.8468	0.7610	0.8952
	Sagittal -64 (15%)	0.4808	0.5616	0.8441	0.8003	0.8768

TABLE -3 PSNR comparison for perona-malik model, self-snake model, nonlocal means, TV-ROF model and proposed model for rician noise corrupted brain magnetic resonance images.

Modality	Slice/Noise level	Self-snake	Perona-Malik	Nonlocal means	TV-ROF	Proposed Model
T1-weighted	transverse-55 (10%)	18.9073	22.2435	30.3852	32.8754	35.1619
	transverse-55 (15%)	19.7320	23.2769	28.6867	31.3885	33.5143
T1-weighted	transverse-69 (10%)	20.5831	22.9230	30.8812	33.3433	34.4658
	transverse-69 (15%)	20.2350	22.4040	26.8884	30.4625	30.4869
T2-weighted	Coronal-67 (10%)	21.2482	22.1694	25.9446	29.0323	29.7941
	Coronal-67 (15%)	20.8966	22.4176	25.1335	26.3274	26.8026
T2-weighted	Sagittal-84 (10%)	16.5027	22.1631	26.8262	30.9716	32.1781
	Sagittal-84 (15%)	16.7555	23.2785	25.2645	28.4651	28.0697
PD-weighted	transverse-64 (10%)	17.4738	20.2082	25.9456	27.9979	28.5296
	transverse-64 (15%)	17.5916	19.3665	22.9762	23.2581	24.2840
PD-weighted	Sagittal-64 (10%)	14.5507	19.0951	23.2714	25.6401	26.6356
	Sagittal -64 (15%)	15.1156	19.6809	21.1692	23.1255	20.4818

TABLE -4 FSIM comparison for perona-malik model, self-snake model, nonlocal means, TV-ROF model and proposed model for rician noise corrupted brain magnetic resonance images.

Modality	Slice/Noise level	Self-snake	Perona-Malik	Nonlocal means	TV-ROF	Proposed Model
T1-weighted	transverse-55 (10%)	0.8565	0.8621	0.9436	0.9497	0.9815
	transverse-55 (15%)	0.8358	0.8308	0.9389	0.9508	0.9804
T1-weighted	transverse-69 (10%)	0.8390	0.8554	0.9316	0.9391	0.9772
	transverse-69 (15%)	0.8229	0.8111	0.9314	0.9384	0.9763
T2-weighted	Coronal-67 (10%)	0.8453	0.8596	0.9273	0.9405	0.9763
	Coronal-67 (15%)	0.8164	0.8364	0.9234	0.9355	0.9745
T2-weighted	Sagittal-84 (10%)	0.8440	0.8787	0.9376	0.9546	0.9818
	Sagittal-84 (15%)	0.8189	0.8498	0.9332	0.9524	0.9775
PD-weighted	transverse-64 (10%)	0.8081	0.8162	0.9158	0.9167	0.9677
	transverse-64 (15%)	0.7673	0.7645	0.9152	0.9114	0.9658
PD-weighted	Sagittal-64 (10%)	0.7786	0.8023	0.9178	0.9073	0.9673
	Sagittal -64 (15%)	0.7418	0.7621	0.9169	0.9107	0.9544

TABLE – 5 MAE comparison for perona-malik model, self-snake model, nonlocal means, TV-ROF model and proposed model for rician noise corrupted brain magnetic resonance images.

Modality	Slice/Noise level	Self-snake	Perona-Malik	Nonlocal means	TV-ROF	Proposed Model
T1-weighted	transverse-55 (10%)	26.7403	17.8043	5.7336	4.3333	3.2415
	transverse-55 (15%)	23.6213	15.0556	7.0900	5.0586	3.7520
T1-weighted	transverse-69 (10%)	21.6645	16.4206	5.4028	4.0323	3.6584
	transverse-69 (15%)	22.1466	16.8208	8.7500	5.7304	5.8004
T2-weighted	Coronal-67 (10%)	19.6359	17.6339	8.3136	6.1917	5.7506
	Coronal-67 (15%)	19.2307	14.3109	9.4163	8.5844	8.3494
T2-weighted	Sagittal-84 (10%)	35.4803	17.6224	7.5367	4.9697	4.5780
	Sagittal-84 (15%)	34.0533	14.3241	9.3645	6.8341	7.3172
PD-weighted	transverse-64 (10%)	32.3348	22.9958	9.6304	7.6477	7.5582
	transverse-64 (15%)	31.2467	24.8262	13.7285	13.0546	11.7736
PD-weighted	Sagittal-64 (10%)	44.6690	26.5114	13.1873	12.0372	9.2879
	Sagittal -64 (15%)	42.3315	23.1104	16.9389	13.6376	18.4209

The experimental results prove that the adaptive version of the proposed model enables the preservation of important image features such as edges, corner and textures also concurrently suppresses noise. In the model setting the variable exponent $\alpha(|\nabla u|)$ to 1 at image edges makes the image regularized by TV norm that is the

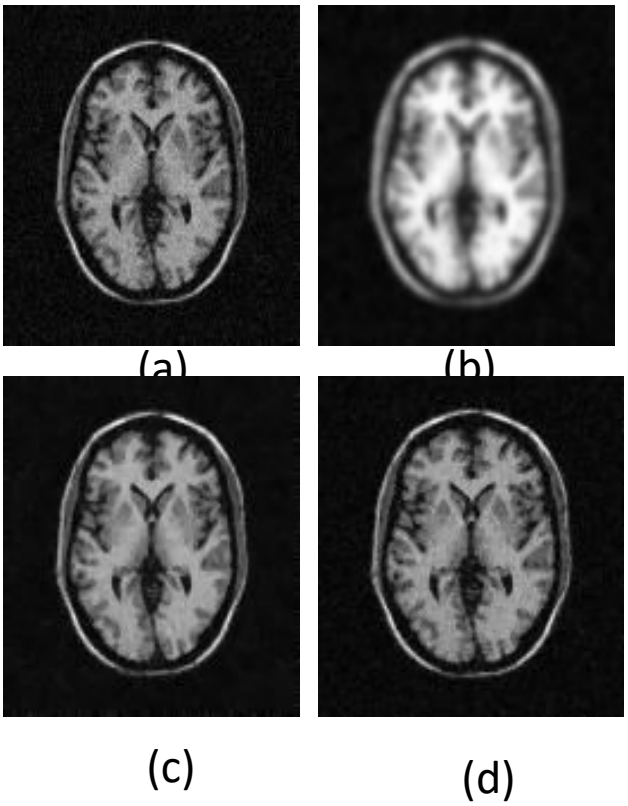

Fig.5 (a) T1-weighted transverse-55 MRI slice with 10% rician noise level (b) denoised image using α =2 (Tikhonov)) (c) denoised image using α = 1(TV-ROF). (d) denoised image using adaptive $\alpha(|\nabla u|)$

gradient of an image this enables edge recovery and setting the variable exponent $\alpha(|\nabla u|)$ to 2 in the flat ramp region makes the image regularized by square of the gradient this promotes strong noise removal. When $\alpha(|\nabla u|)$ is used as constant with value 1 then the model is TV-ROF model preserves edges well. When $\alpha(|\nabla u|)$ is used as a constant with value 2 then the model is Tikhonov model enbles strong smoothing. In Figs. 5-6 we could notice that when adaptively changing $\alpha(|\nabla u|)$ produces better quality image rather using fixed value of 1 or 2. Adaptively changing $\alpha(|\nabla u|)$ produces denoised images having higher values of peak signal to noise ratio(PSNR), structural similarity index measure(SSIM), feature similarity index measure(FSIM) and lower value of Mean average error (MAE) compared to constant 2 and 1 that is compared to Tikhonov model and TV-ROF model. The quality metrics presented in Table 1 also proves this fact. Since the metric MAE is more sensitive to distortion than Mean square error(MSE), the metric MAE is computed to measure how efficient the algorithm is in edge preservation[33].

Quantitative analysis also confirms that adaptive regularization model is superior since it produces higher values of quality metrics. Table 2 shows the proposed method generates higher SSIM values in comparison with other models, which means that denoised image is highly similar to the original image. Table 3 shows the value of PSNR quality metric for different brain MR images of different modality. The proposed algorithm performs best since it achieves maximum PSNR values for most of the brain MR images compared to conventional methods. This finding agrees with the visual quality of images generated by the proposed algorithm .

The images processed by the proposed algorithm are sharper and have clear and thicker edges also there is no contrast loss. In addition there is no blocking or staircasing effect and texture of image is also preserved. Table 4 shows that the proposed algorithm can able to attain a visually enhanced image compared to other methods which is proved from the higher values of FSIM quality metric. An important thing we notice from Table 5 is that mean absolute error is very minimum for the images produced by the proposed algorithm compared to other conventional diffusion methods.

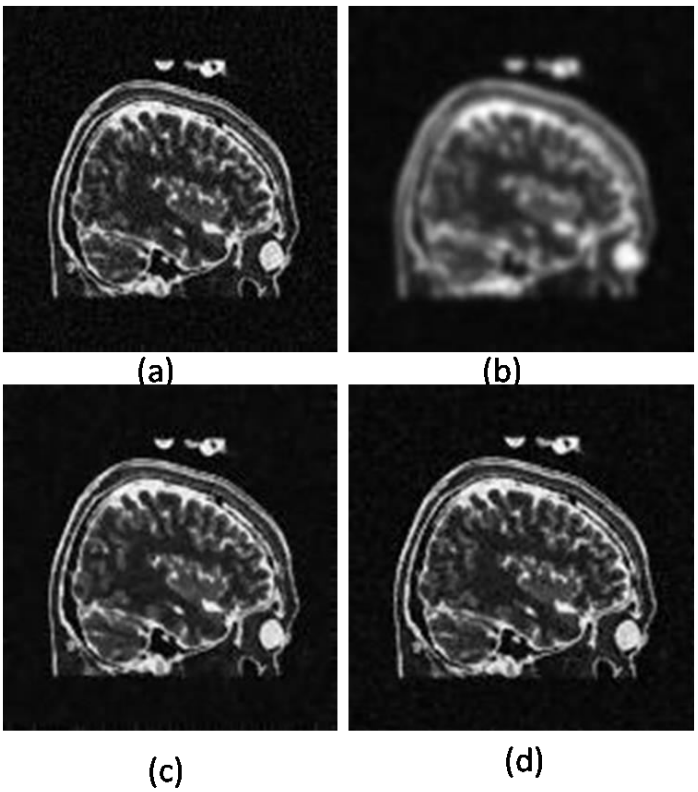

Fig.6 (a) T2-weighted sagittal slice 84 10% rician noise level (b) denoised image using α =2 (Tikhonov) (c) denoised image using α =1(TV-ROF) (d) denoised image using adaptive $\alpha(|\nabla u|)$.

The TV-ROF model's performance comes next to our proposed method. Visually these two methods produces nearly same quality images. However, the experimental results proves that the proposed method performs best for most of the images except brain MR image slice PD-weighted sagittal-64 having rician noise level 15%. For this image the proposed method achieves lesser PSNR value and higher MAE compare to TV-ROF model. For all other MR image slices proposed algorithm achieves higher values for PSNR, SSIM and FSIM. The proposed algorithm generates lesser mean absolute error compared to all other methods for most of the images. This could be noticed in tables 2-5. The performance of conventional self-snake diffusion algorithm is worst among all. Next lower performance algorithm is conventional perona-malik diffusion. Performance of non-local means algorithm takes third place.

The proposed algorithm is found to be very efficient in removing salt and pepper noise also. The salt and pepper noise corrupted standard images are denoised using proposed algorithm as well as other diffusion algorithms such as self-snake model, perona-malik model, non-local means algorithm and TV-ROF model. The visual quality of denoised images produced by various algorithms are compared in Fig 7 and Fig. 8. For salt and pepper noise corrupted standard images also the visual quality of denoised image produced by the proposed algorithm is found to be of best quality compared to other algorithms. The quality metrics such as PSNR, MAE, SSIM and FSIM are computed for denoised images produced by various algorithms for salt and pepper noise corrupted standard images. The quality metrics are presented in the tables 6-9. The proposed algorithm generates highest quality metric values for PSNR, FSIM and SSIM compared to other models for salt and pepper noise corrupted standard images also. The proposed algorithm produces lowest mean average error (MAE) compared to other diffusion algorithms.

Table 6 SSIM comparison for perona-malik model, self-snake model, nonlocal means, TV-ROF model and proposed model for salt and pepper noise corrupted standard images.

Image	Nonlocal means	Perona-Malik	Self-snake	TV-ROF	Proposed Model
Cameraman	0.79	0.63	0.70	0.82	0.87
Lena	0.82	0.73	0.80	0.85	0.90
Wheel	0.84	0.71	0.77	0.85	0.89
Liftingbody	0.74	0.65	0.71	0.75	0.82
coins	0.80	0.70	0.77	0.80	0.86

Table 7 PSNR comparison for perona-malik model, self-snake model, nonlocal means, TV-ROF model and proposed model for salt and pepper noise corrupted standard images.

Image	Nonlocal means	Perona-Malik	Self-snake	TV-ROF	Proposed Model
Cameraman	26.51	21.59	22.41	27.71	28.42
Lena	27.49	25.17	26.40	28.55	30.04
Wheel	25.79	18.50	18.83	22.11	28.05
Liftingbody	27.46	24.51	25.15	27.36	28.48
coins	27.04	21.33	23.87	26.56	28.31

Table 8 FSIM comparison for perona-malik model, self-snake model, nonlocal means, TV-ROF model and proposed model for salt and pepper noise corrupted standard images.

Image	Nonlocal means	Perona-Malik	Self-snake	TV-ROF	Proposed Model
Cameraman	0.91	0.84	0.88	0.93	0.97
Lena	0.93	0.88	0.91	0.95	0.96
Wheel	0.97	0.90	0.91	0.96	0.98
Liftingbody	0.92	0.87	0.89	0.91	0.94
Coins	0.91	0.87	0.90	0.93	0.95

Table 9 MAE comparison for perona-malik model, self-snake model, nonlocal means, TV-ROF model and proposed model for salt and pepper noise corrupted standard images.

Image	Nonlocal means	Perona-Malik	Self-snake	TV-ROF	Proposed Model
Cameraman	4.18	13.39	11.91	3.11	1.91
Lena	4.17	6.05	5.49	2.96	1.69
Wheel	5.06	25.70	25.36	16.15	2.47
Liftingbody	2.96	7.66	6.822	3.15	2.01
coins	2.85	15.01	9.26	3.20	1.55

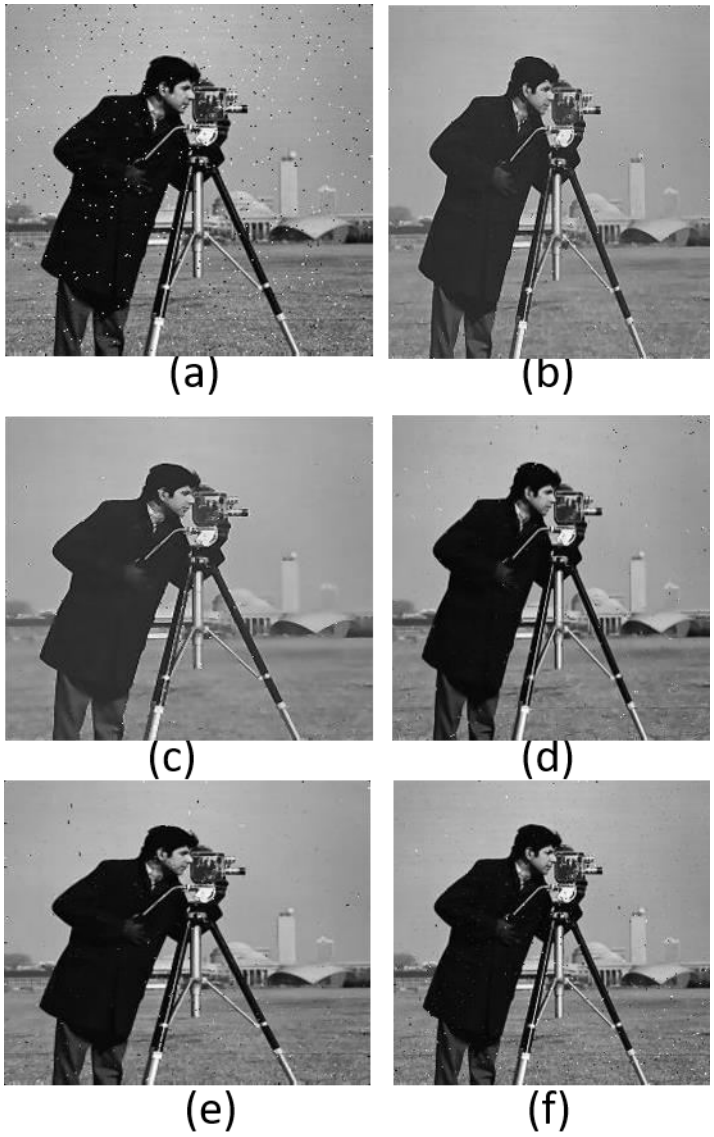

Fig.7 (a) cameraman image with salt and pepper noise with density 0.01 (b) denoised image by self-snake model (c) denoised image by perona-malik model (d) denoised image by non-local means algorithm (e) denoised image by TV-ROF (f) denoised image by proposed algorithm.

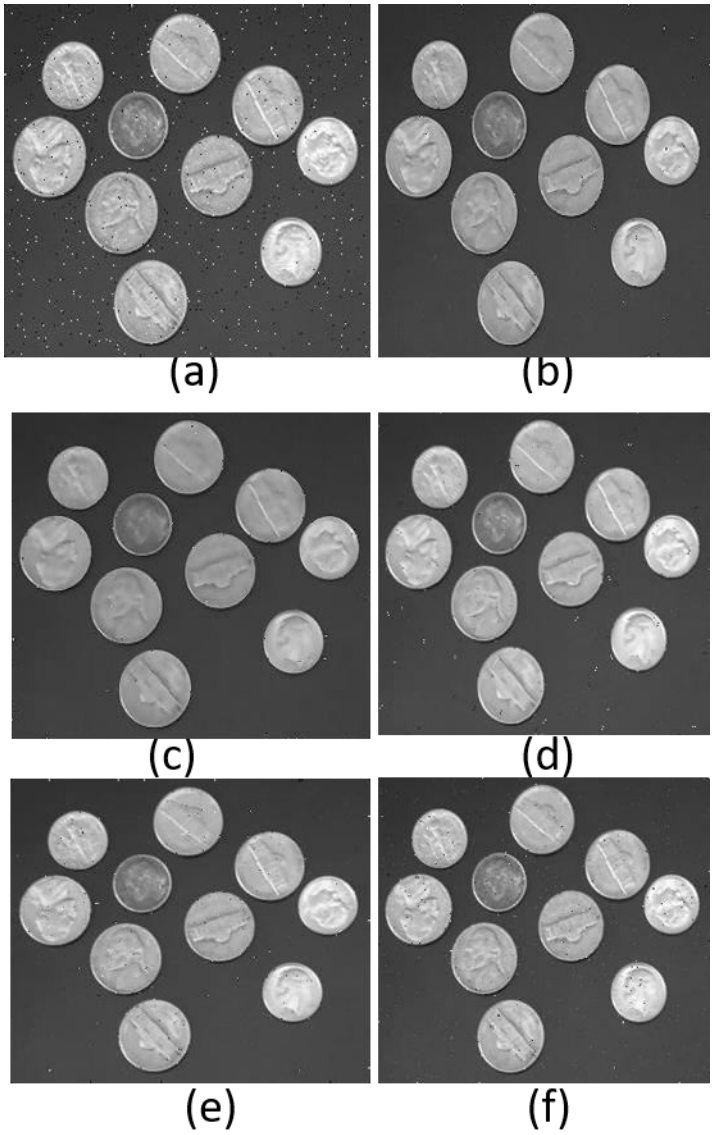

Fig.8 (a) coins image with salt and pepper noise with density 0.01 (b) denoised image by self-snake model (c) denoised image by perona-malik model (d) denoised image by non-local means algorithm (e) denoised image by TV-ROF (f) denoised image by proposed algorithm.

5. Conclusions

To overcome the drawbacks of conventional total variation regularization model such as TV-ROF model and Tikhonov model the adaptive variable exponent based total variation regularization model is proposed which uses a variable exponent based on an edge stopping function in the regularization term and the weight of the fidelity term is also adaptive. The performance of proposed adaptive total variation regularization algorithm is analyzed by denoising rician noise corrupted brain MR images for varying noise levels and also by denoising salt and pepper noise corrupted standard images. The performance is evaluated in terms of MAE, PSNR, FSIM and SSIM for rician noise. Experimental results show that the proposed algorithm performs best compared with other methods such as classical perona-malik filter, self-snake filter, total variation- ROF model, Tikhonov model and nonlocal means filter both qualitatively as well as quantitatively. The research work can be extended in the direction using different numerical algorithms for solving the functional such as duality based splitting method and alternating minimization method.

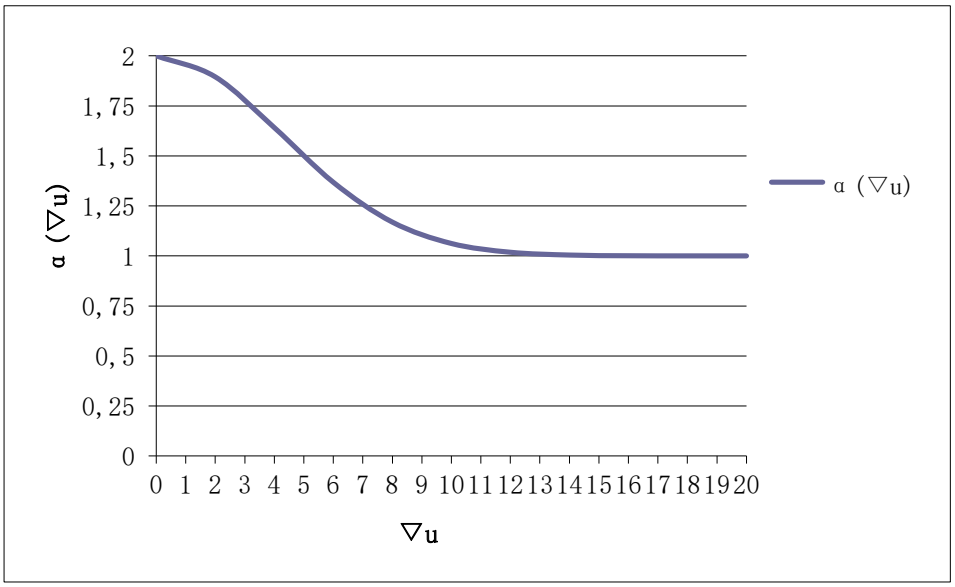

Fig. 7 Value of local feature dependent variable exponent α(|▽u|) with respect to the gradient ▽u

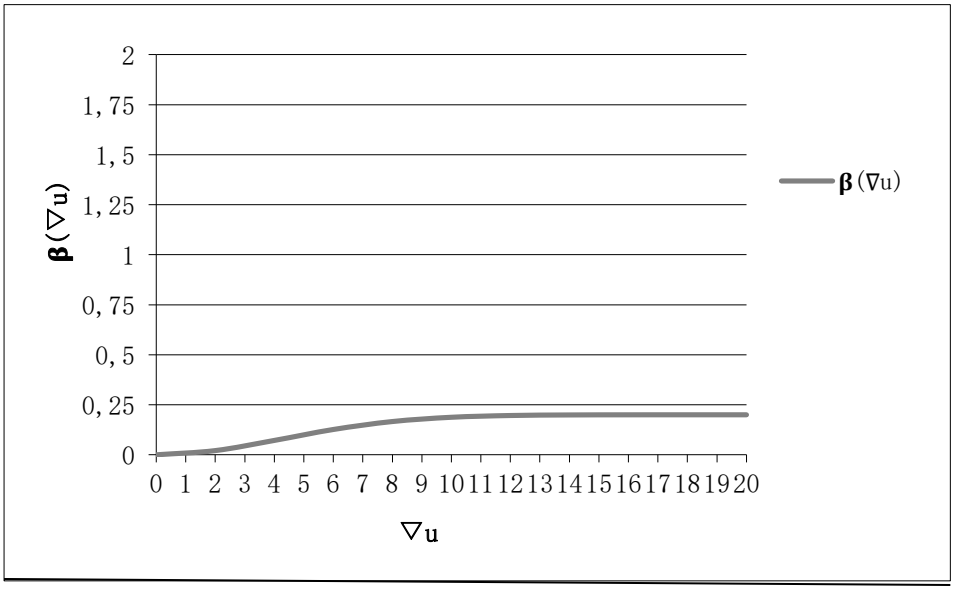

Fig. 8 Value of local feature dependent regularization parameter β(|▽u|) with respect to the gradient ▽u

References

1.T.Chan, Jianhong Shen, L. Vese. : Variational PDE models in image processing. DOI:10.21236/ada437477
2. Wang YY, Wu SY.: Adaptive Image Denoising Approach Based on Generalized Lp Norm Variational Model. Applied Mechanics and Materials May 2014;556–562:4851–4855. https://doi.org/10.4028/www.scientific.net/amm.556-562.4851.
3. Dali Chen, Yang Quan Chen Dingyu Xue.: Fractional-order total variation image denoising based on proximity algorithm. Applied Mathematics and Computation, Volume 257 Issue April 2015 pp 537–545https://doi.org/10.1016/j.amc.2015.01.012
4. Qiang Chen, Philippe Montesinos , Quan Sen Sun , Peng Ann Heng , De Shen Xia.: Adaptive total variation denoising based on difference curvature. Image and Vision computing, Vol. 28, Issue 3, pp. 298-306, 2010.
5. Kui Liu, Jieqing Tan, and Benyue Su.: An adaptive Image Denoising Model based on Tikhonov and TV Regularizations. Advances in Multimedia, Vol. 2014, Article ID 934834.

6. S. Osher, M. Burger, D. Goldfarb, J. Xu, W. Yin.: An iterative regularization method for total variation based on image restoration. Multiscale Modeling and Simulation 4 (2) (2005) 460–489.
7. M. Nikolova.: Minimizers of cost-functions involving non smooth data-fidelity terms. SIAM Journal on Numerical Analysis 40 (3) (2002) 965–994.
8. T. Chan, S. Esedoglu.: Aspects of total variation regularized L1 function approximation. SIAM Journal of Applied Mathematics 65 (5) (2005) 1817– 1837.
9. S. Esedoglu, S. Osher.: Decomposition of images by the anisotropic Rudin–Osher–Fatemi model. Communications in Pure and Applied Mathematics 57 (12) (2004) 1609–1626.
10 P. Blomgren, P. Mulet, T. Chan, C. Wong.: Total variation image restoration numerical methods and extensions. In ICIP, Santa Barbara, 1997, pp. 384–387.
11 G. Gilboa, Y.Y. Zeevi, N. Sochen.: Texture preserving variational denoising using an adaptive fidelity term. In Proceedings of the VLSM, Nice, France, 2003, pp.137–144.
12. P. Blomgren, T.F. Chan, P. Mulet.: Extensions to total variation denoising. In Proceedings of SPIE, San Diego, vol. 3162, 1997.
13. Yadav R B , Srivastava S, Srivastava R.: A partial differential equation based general framework adapted to Rayleigh's, Rician's, and Gaussian's distributed noise for restoration and enhancement of magnetic resonance image. Journal of Medical Physics. Vol. 41, Issue 4, pp. 254-265, 2016.
14. V. Kamalaveni, S. Veni, K. A. Narayanankutty. : Improved Self-snake based Anisotropic Diffusion Model for Edge Preserving Image Denoising using Structure Tensor. Multimedia Tools and Applications. Springer, 2017.
15. Qiangqiang Yuan, Liangpei Zhang, Senior Member, IEEE, and Huanfeng Shen, Member, IEEE.: Hyperspectral Image Denoising Employing a Spectral–Spatial Adaptive Total Variation Model. IEEE Transcations on Geoscience and Remote Sensing. 2012.
16. V.Kamalaveni, K.A.Narayanankutty, S.Veni .: Performance Comparison of Total Variation Based Image Regularization Algorithms. International Journal on Advanced Science Engineering and Information Techology. Vol. 6, No.4,2016.
17. Junfeng Yang et. al. : An efficient TV-L1 algorithm for deblurring multichannel images corrupted by impulsive noise. SIAM J. SCI. COMPUT. Society for Industrial and Applied Mathematics Vol. 31, No. 4, pp. 2842–2865
18. Amir Beck and Marc Teboulle. : Fast Gradient-Based Algorithms for Constrained Total Variation Image Denoising and Deblurring Problems. IEEE Transactions on Image Processing, 2009.
19. Yang Wang and Haomin Zhou.: Total Variation Wavelet Based Medical Image Denoising. International Journal of Biomedical Imaging, 2006.
20. I.Rudin, S. Osher, and E. Fatemi.: Nonlinear total variation based noise removal algorithms. Physica D: NonlinearPhenomena, 60(1):259–268, 1992.
21. Fenlin Yang, Ke Chen and Bo yu.: Adaptive Second Order Variational Model for Image Denoising. International Journal of Numerical Analysis and Modelling, Volume 5, No.1. pages. 85-98, 2014.
22. Aditya Chopra, Heng Lian.: Total Variation, adaptive total variation, and nonconvex smoothly clipped absolute deviation penalty for denoising blocky images. Pattern recognition, 2010.
23. Li Guo, Weilong Chen, Yu Liao, Honghua Liao, and Jun Li.: An edge-preserved an image denoising algorithm Based on Local Adaptive Regularization. Hindawi Publishing Corporation, Journal of Sensors, Volume 2016, Article ID 2019569, 6 Pages, 2016, http://dx.doi.org/10.1155/2016/2019569
24. Chan T.F., Chen K., Tai XC.: Nonlinear Multilevel Schemes for solving the Total Variation Image Minimization Problem. Image Processing Based on Partial Differential Equations. Mathematics and Visualization. Springer, Berlin, Heidelberg, 2007.
25. You Y. L., Kavesh M.: Fourth-order partial differential equations for noise removal. IEEE transcations on image Processing, Vol. 9, No.10, 1723-1730, 2000.
26. P. Charbonnier, L. Blanc-Feraud, G. Aubert, and M. Barlaud. : Deterministic edge preserving regularization in computed imaging. IEEE Transactions on Image Processing, 6(2):298–311, 1997.
27. Zhichang Guo, Jiebao Sun, Dazhi Zhang and Boying Wu.: Adaptive Perona–Malik Model Based on the Variable Exponent for Image Denoising. IEEE Transcations on Image Processing, Vol. 21, No.3, March 2012.
28. Wang Y.Q., JichangGuo, WufanChen and Wenxue Zhang.: Image denoising using Modified Perona–Malik Model based on Directional Laplacian. Signal Processing 93 (2013) 2548–2558.
29. Liming Tang and Zhuang Fang.: Edge and contrast preserving in total variation image denoising. EURASIP Journal on Advances in Signal Processing, 2016. DOI 10.1186/s13634-016-0315-5.
30. Antoni Buades et al.: A non-local algorithm for image denoising. In Proceeding CVPR'05 Proceedings of the 2005 IEEE Computer Society Conference on Computer Vision and Pattern Recognition- Volume 2 – Pages 60-65, 2005.
31. Sachin kumar S, Neethu Mohan, K.P.Soman, Prabaharan P.: Total Variation Denoising Based Approach for R-peak Detection in ECG Signals. **D**ecember 2016, Procedia Computer Science 93:697-705,DOI:10.1016/j.procs.2016.07.26
32. S.Karthik, Hemanth VK, K.P. Soman, V.Balaji, Sachin Kumar S, M. Sabarimalai Manikandan : Directional Total Variation Filtering Based Image Denoising Method. International Journal of Computer Science Issues, Vol. 9, Issue 2, No 1, March 2012, ISSN (Online): 1694-0814.
33. Fabrizio Rosso: Performance Evaluation of Noise Reduction Filters for Color Images through Normalized Color Difference(NCD) Decomposition. ISRN Machine Vision, Volume 2014, Article ID 579658.